Synaptic Plasticity Powering Long-Afterglow Organic Light-Emitting Transistors

Yusheng Chen, Hanlin Wang, Yifan Yao, Ye Wang, Chun Ma, Paolo Samorì

DOI: 10.1002/((please add manuscript number))

Article type: Communication

Synaptic Plasticity Powering Long Afterglow Organic Light-Emitting Transistors

Yusheng Chen, Hanlin Wang, Yifan Yao, Ye Wang, Chun Ma, Paolo Samorì*

Y. Chen, Dr. H. Wang, Dr. Y, Yao, Y. Wang, Dr. C. Ma, Prof. P. Samorì
Université de Strasbourg, CNRS, ISIS
8 allée Gaspard Monge
67000 Strasbourg, France
E-mail: samori@unistra.fr

Keywords: long afterglow, synaptic transistors, organic light-emitting transistors, thermally activated delayed fluorescence

Abstract:

Long-lasting luminescence in opto-electronic devices is highly sought after for applications in optical data storage and display technology. While in light-emitting diodes this was achieved by exploiting long afterglow organic materials as active components, such strategy was never pursued in light-emitting transistors, that are still rather unexplored and whose technological potential is yet to be demonstrated. Herein, we report on the fabrication of long afterglow organic light-emitting transistors (LAOLETs) whose operation relies on an unprecedented strategy based on a photo-induced synaptic effect in an inorganic indium-gallium-zinc-oxide (IGZO) semiconducting channel layer, to power a persistent electroluminescence in organic light-emitting materials. Oxygen vacancies in the IGZO layer, produced by irradiation at λ=312 nm, free electrons in excess yielding to a channel conductance increase. Due to the slow recombination kinetics of photo-generated electrons to oxygen vacancies in the channel layer, the organic material could be fuelled by post-synaptic current and displayed a long-lived light-emission (hundreds of seconds) after ceasing UV irradiation. As a proof-of-concept, our LAOLETs were integrated in active-matrix light-emitting arrays operating as visual UV sensors capable of long-lifetime green light emission in the irradiated regions.

.

Organic light-emitting transistors (OLETs) have gained a notable attention during the last few years as opto-electronic functional element for the fabrication of the next generation of active-matrix display. OLETs indeed simultaneously integrates the functions of light-emission, gate-modulated electrical switching and optically switchable operation modes. Such multifunctional nature is instrumental for smart display technologies.[1] Upon conversion of triplet excitons into singlet excitons via "reverse intersystem crossing", thermally activated delayed fluorescence (TADF) materials can harvest energy electrons from both the singlet and triplet states thereby contributing to light-emission. Such unique class of materials are regarded as ideal candidates for low-cost and highly efficient light-emitting devices.[2] During the last few years, high-performance OLETs with high external quantum efficiencies based on TADF materials have been reported.[3]

Organic afterglow, also called persistent photoluminescence, is a well-known long-lived emission phenomenon in which photoluminescence of the pure organic materials can persists for several seconds after light irradiation is ceased.[4] Organic afterglow emitting materials have raised quite some interests in view of their potential application in the optical data storage, sensors, in-vivo imaging and anti-counterfeiting.[5] However, many are the challenges limiting the practical applications of organic afterglow, including the light-emitting colour tunability, lifetimes of organic luminescence and phosphorescence quantum yield. Moreover, the need for stringent molecular design principles, e.g. promoting H-aggregates in solid state to stabilize the generated triplet exciton, jeopardizes the implementation of a long afterglow function in organic opto-electronic devices.[6]

Persistent photoconductivity (PPC) is another delayed response phenomenon common in opto-electronics which can be found in devices comprising various types of amorphous metal oxide semiconductors such as InZnO (IZO), InGaZnO (IGZO), and ZnSnO (ZTO).[7] Due to the dynamic nature of the process relying on the ionization of oxygen vacancies, electron density is increased upon the irradiation of UV photons thus increasing the conductance of these materials. After ceasing the UV irradiation, conductance slowly decreases going gradually through low resistance states due to the slow recombination rate of electrons and oxygen vacancies.[8] Since this behavior highly resembles the plasticity phenomenon in biological synapses or neural systems, metal oxide semiconductors can be potentially exploited as active layers in the fabrication of artificial synaptic field-effect transistors to attain a short- and long-term memory.[9]

Here we report for the first time a long afterglow organic light-emitting field-effect transistor (LAOLETs). The device architecture relies on an IGZO field-effect transistor (FET) possessing

synaptic characteristics. In particular, the IGZO channel has been designed to feature post-synaptic current flow capable of driving the light-emission. Synaptic plasticity is realized by generating oxygen vacancies in IGZO via UV irradiation, leading to slow electron-oxygen vacancy recombination kinetics. Moreover, synaptic characteristics of solution processed IGZO are investigated and tuned by varying the concentration of In atoms, thereby optimizing IGZO thin-film function as channel layer with a long-term potentiation property. Subsequently, TADF organic light-emissive layers have been deposited onto the IGZO channel yielding an area light-emission. We demonstrate that synaptic behaviour of IGZO is retained after deposition of the organic light-emissive layer. Significantly, our devices display electroluminescence with a unique synaptic property. By varying the gate bias, our LAOLETs exhibit persistent light-emission featuring variable lifetime after exposure to UV stimulus. In absence of an applied gate voltage, such a synaptic-plasticity facilitated afterglow emission has a lifetime exceeding 270 s, after 50 s UV irradiation. In contrast to conventional long afterglow devices requiring specific design of room-temperature phosphorescence materials, our strategy makes use of electronic means arising from oxygen-vacancies in metal-oxides, to achieve similar device functions. Finally, time-dependent synaptic-type afterglow in LAOLETs is displayed and systematically characterized.

An amorphous metal-oxide thin films have been employed not only as *n*-type channel layer but also memory function layer due to their high mobility and PPC characteristic. Upon UV irradiation, electrons present in excess on the IGZO surface absorb energy to be released into the bulk. This process is generally attributed to the ionization of oxygen vacancies (single charged ($V_O \rightarrow V_O^+ + e^-$) or double charged (or $V_O \rightarrow V_O^{2+} + 2e^-$)), as illustrated in Figure 1a. This increase in electron density leads to the upshift of the Femi level (E_F) of IGZO, which in turn effectively reduces the injection barrier height between IGZO and metal (Al) contacts. In this way, IGZO based FETs can persistently retain their low resistance state without the application of a gate bias, as a result of the slow neutralization or recombination rate of released electron with oxygen vacancies.

Long afterglow organic light-emitting field-effect transistors (LAOLETs) have been fabricated with a lateral IGZO channel and a vertically-stacked organic emissive layer. Figure 1b portrays the architecture of Si/SiO_2/IGZO/Al/poly[9,9-bis(60-(N,N-diethylamino) hexyl)-fluorene-alt-9,9-bis(3-ethyl(oxetane-3-ethyoxy)-hexyl)-fluorene] (PFNOX)/light-emission layer/N,N′-Di(1-naphthyl)-N,N′-diphenyl-(1,1′-biphenyl)-4,4′-diamine (NPB)/Au. The light-emission layer comprises 9,10-bis(4-(9H-carbazol-9-yl)-2,6-dimethylphenyl)-9,10-diboraanthracene (CzDBA) as a TADF green light-emitting material hosted in a 4,4-bis(N-

carbazolyl)-1,1-biphenyl (CBP) matrix.[10] To balance of electron and hole charge carrier concentration in emission layer, PFNOX and NPB were employed as electron and hole transporting layer, respectively. Complementary electrodes were deposited through aligned shadow masks and optical images of typical device were captured (Figure S1, Supporting Information). The energy levels and chemical structures of these materials are displayed in Figure 1c and 1d, respectively.

Firstly, transistors containing a mono-component IGZO layer as active material were fabricated to explore the synaptic behaviour of IGZO. A bottom-gate, top-contact geometry, denoted as Si/SiO_2/IGZO/Al, was chosen. The IGZO layer with a thickness of ~20 nm was deposited through sol-gel method on the Si substrate covered with a 230 nm thick layer of thermally grown SiO_2. A formulation of metal precursors made of indium nitrate, gallium nitrate, and zinc acetate were dissolved in 2-methoxyethanol, respectively. 50 nm Al layer as top contacts was deposited through a shadow mask by thermal evaporation, serving as interdigitated source and drain electrodes.

The solution-processing of IGZO has the advantage that the atom ratio of the metal ion in the amorphous metal oxide can be optimized easily by tuning the mixing ratio of the precursor in the solution. Atom ratio of Ga and Zn were kept at 1:1, and the percentage of In was varied from 50%, 65% to 80%. Atomic force microscopy (AFM) topographical images revealed an ultra-smooth surface of the IGZO film with a root-square-mean roughness (R_{RMS}) of about 0.2 nm as determined in an area of 5 × 5 μm^2. The ultra-flatness of this surface is potentially advantageous for multilayer stack formation (Figure S2, Supporting Information). Transfer curves of IGZO-based transistors recorded by using different indium content are displayed in Figure 2a (Figure S3, Supporting Information), whereas the key performance indicators of all the devices are summarized in the Table S1. We found that the atom ratio of indium in IGZO film strongly influences the device performance, including its threshold voltage (V_{Th}), its electron mobility and its light response behaviour.[11] When irradiated for 5 second with a 312 nm UV light, IGZO films with low-indium-ratio (50%) did not show any obvious V_{Th} shift and current change, whereas IGZO films with 65% and 80%-In content exhibited a negative shift of the V_{Th}. However, before UV irradiation, high-indium-ratio (80%) IGZO films showed a notable negative shift of V_{Th} while the changes of the off-state current were modest. For IGZO films with In ratio of 65%, the V_{Th} is positioned ca. at 0 V, thus allowing the device to be fabricated as two-terminal memory resistors as a comparative device for control experiments. Hence, 65%-In IGZO films were chosen in order to exploit its synapse behaviour when integrated in LAOLETs. Normalized different gate-bias time-dependent measurement of the

65%-In IGZO-based transistors after UV light illumination were also measured and shown in Figure 2b. The lifetime (τ_i) of the devices can be determined from the decay curves according to the exponential equation $I(t) = I_0\, e^{-t/\tau_i} + I_\infty$, where I_0 is the initial current and I_∞ is the steady-state current. Under zero gate bias, the current undergoes a slow kinetics decay from on-state to off-state (baseline), with a lifetime of 190 s (Figure S4a, Supporting Information). Conversely, when a gate voltage of −20 V and −40 V was applied we observed a negative gate bias induced faster current decay whose lifetime amounts to 118 s and 88.5 s, respectively (Figure S4b and S4c, Supporting Information).[12] These changes in the decay dynamics of on-state currents clearly demonstrate that the synaptic relaxation behaviour as well as V_{Th} can be well tuned by varying the indium ratio in the precursor solution and the operation gate voltage.

After prolonged exposure time to UV irradiation, transfer curves of 65%-In IGZO-based transistor were immediately measured for comparison. Transfer curves of this transistor before and after UV irradiation are displayed in Figure 2c. The relevant devices parameters are summarized in Table 1. Upon the exposure to UV light the field-effect mobilities exhibited a modest yet gradual increase from 0.151 to 0.358 $cm^2\ V^{-1}\ s^{-1}$. On the same time, V_{Th} shifted gradually towards negative value, from 4.86 V to −111 V, and the I_{on}/I_{off} ratio of device decreased correspondingly. This observation provides evidence that the enhanced-mode FET operation can be converted into depletion-mode upon 25 s exposure to 312 nm UV light with an increase of the I_{DS} (at V_G = 0 V) up to magnitude of 10^{-3} A. For the sake of comparison, the pristine IGZO in its off-state (at zero gate bias) displays I_{DS} of a few picoampere.

Synaptic plasticity is one of most crucial characteristics for synaptic devices and it is associated with short- and long-term memory.[13] Decaying characteristics of post-synaptic current (PSC) with one UV-stimulus and five UV-stimulus are portrayed in Figure 2d. When a single 5 seconds lasting irradiation of 312 nm UV light with an intensity of 3 $\mu W\ mm^{-2}$ was applied, the synaptic device exhibited short-term plasticity (STP) with a rapid decay of the PSC to its steady-state after the UV stimulus on the few tens of seconds timescale (enlarged figure, show in Figure S5). However, when five UV light irradiations with the same intensity and width at intervals of 1 min were applied, the device displayed long-term plasticity (LTP) behaviour, with the high-current state persisting for a longer period of time (280 s, Figure S4d, Supporting Information). These observations can be attributed to the slow recombination kinetics of such electrons with oxygen vacancies, thereby producing an accumulated or high density of free electrons in the channel. This finding is in line with literature showing that the adjustment of memory behaviour can be controlled by varying the exposure time to UV light.[11,14] Such a

LTP behaviour of the transistor provides the tool to power the light emitting material for a long-lasting emission.

The synaptic memory behaviour of IGZO was observed also in the multi-layer LAOLETs devices. Device Electrical and optical output curves are portrayed in Figure 3a where the applied gate voltages (V_G) ranged from −60 V to 60 V and drain voltages (V_{DS}) was swept from −20 V to 40 V. The width (W) and length (L) of the channel amounted to 27×10^3 μm and 200 μm, respectively, whereas the emission area was defined as 4.22 mm^2. The brightness of devices was found to increase with the drain-source current. When V_G of 60 V and V_{DS} of 40 V were applied, the brightness reached 196 cd m^{-2}. Photoluminescence spectra of the emission layer and electroluminescence spectra of LAOLETs are displayed (Figure S6a, Supporting Information). The maximum emission peak of photoluminescence (PL) spectra was positioned at 525 nm, while that of electroluminescence spectra was observed at 549 nm. This value corresponds to color coordinates of (0.37, 0.57) from Commission Internationale de l'Eclairage (CIE) (Figure 3c). This slightly redshift in spectra of LAOLETs was caused by the presence of NPB and Au layer (Figure S6b, Supporting Information) which can be further optimized in the future work.

Electrical and optical transfer curves of LAOLETs were measured immediately after 10 second UV oblique irradiation with intensity of 3 μW mm^{-2}. Similar to synaptic transistor based on a neat IGZO layer, V_{Th} of device also displayed a gradual negative shift with the UV irradiation, from −12.0 V to −29.4 V, accompanied by light turn-on voltage (V_{On}) negative shift from 3.0 V to −9.7 V, where V_{On} of the LAOLETs were defined from optical transfer curves by extrapolating the straight line portion of the curves (against the V_G axis, Figure S7 in the Supporting Information). The detailed device parameters are reported in Table 2. Time-dependence PSC and post-synaptic brightness (PSB) of the LAOLETs are displayed in Figure 3b. It reveals a similar PSC trend thus indicating that multi-layer fabrication process did not influence the PPC behavior of the channel layer. More importantly, electroluminescence of LAOLETs and post-synaptic brightness exhibited the similar trend with PSC, characterized by a long-lived emission after the UV light is turned off, providing unambiguous evidence for the afterglow nature of the emission, which presented in Figure 3d. The decay ratio of PSB was attributed to the degeneration of organic emission materials, and it resulted being slightly faster than that of PSC, yet the latter can be optimized after encapsulation or embedding state-of-art light-emission materials.[15] Time dependence measurement of the same LAOLETs device just differing by the absence of the IGZO layer, were carried out (see Figure S8, Supporting Information). The nearly negligible change in current as a result of UV irradiation indicates that

the PSC in our LAOLETs is due to the light-responsive nature of the IGZO layer. Electroluminescence lifetime (τ_l) of LAOLETs can be also determined from the time-resolved decay of luminescent intensity in the exponential decay equation: $L(t) = L_0\, e^{-t/\tau_l} + L_\infty$, where L_0 is the initial fluorescence strength at starting time (t = 0). Under V_G = 0 V, after 50 s UV stimulus, brightness of 11 cd m^{-2} was achieved, and τ_l of 272 s was calculated (Figure S9a, Supporting Information). However, under V_G = −30 V, lower brightness of 4 cd m^{-2} and shorter τ_l of 159 s were observed (Figure 3e and Figure S9b, Supporting Information), which indicates that V_G can be used as a remote control giving access to different decay constants. Moreover, for this kind of LAOLETs, the application of one and five UV irradiation stimuli under both V_G = 0 V and −30 V resulted in STP and LTP, respectively, being consistent with synaptic transistors and also indicating that luminescence efficiency and lifetime can be enhanced upon prolonging the UV irradiation. Time dependent measurement of LAOLETs with input duration five times longer (i.e. amounting to 20 sec) were carried out and the results are presented in Figure S10. While the PSB retention was not prolonged being ruled by the decay of organic emitting materials, the PSC exhibited longer retention times. Compared with room-temperature phosphorescent materials, which is well known that high quantum yield and long lifetime are difficult to be achieved simultaneously,[16] our LAOLETs display a greater technological potential for long afterglow display application. Optical image of LAOLETs under driven voltage before and after UV irradiation are displayed in the Figure 3f.

The persistent light-emission in LAOLETs can also be observed even without applying a gate voltage. To demonstrate this unique behaviour and explore its potential for advanced opto-electronics applications, we have fabricated an *ad hoc* active-matrix light-emitting array composed of 100 two-terminal pixels without gate electrode. As shown in the Figure 4a, the device was fabricated on a 2.5 × 2.5 cm^2 glass substrate with a structure of IGZO/Al/PFNOX/CBP:CzDBA/NPB/Au. Detailed image of the patterned electrode is provided (Figure S11, Supporting Information). The aperture ratio of these devices amounted to 0.39, hence being comparable to that of commercial LED-LCD and OLED displays (around 0.34).[17] After 312 nm UV irradiation through S-shaped shadow mask, channel conductance of stimulated pixels was enhanced, thus leading to PSC. Subsequently, long-lasting light-emission with “S” is observed, demonstrating that our device can function as visual UV sensors with image capturing capability after exposure (Figure S12, Supporting Information). Noteworthy, our unprecedented long afterglow devices do not suffer from undesired appearance of random noise. In fact, the post-synaptic weights difference of each pixels was caused by the different UV photon flux.[18] Optical image of device and shadow masks were captured in Figure 4b, 4c

and Figure S13. Figure 4d also displays the layout of five shadow masks characterized by an *ad hoc* design combining a standard pattern consisting of a number 8 with point defects. Upon exposure of the device successively to five UV irradiations by using a different shadow mask in each of them, it was possible to modulate the photons flux for each pixel thereby enabling to programme coexistence of LTP and STP states in neighbouring pixels. In particular, PSC of STP is not sufficient to power the light-emission of the pixels and PSB with a pattern "8" in absence of noise is observed by the camera. Thus, high luminescence efficiency and long light-emission lifetime were achieved simultaneously under prolonged or repetitive UV stimulus, with a marked difference in brightness between desired area and noise information by an accurate spatial distribution of UV-exposed pixels. As a proof-of-concept, our LAOLETs array possesses a capability of delayed luminescence as an UV-imager due to its synaptic characteristics. The recorded video of this device in action is provided in Supplementary Movie. S1. It is interesting to note that when IGZO layer was embedded in a vertically stacked LED structure (Figure S14, Supporting Information), since the charge transport occur in a shorter channel (about 20 nm) of IGZO, it was not possible to record an appreciable influence to UV irradiation most likely due to the influence of tunneling effect, which results in low On/Off ratios of both current and light emission.

In summary, a synaptic IGZO layer was integrated in a novel LET device architecture to power electroluminescence of solution processed TADF emissive layers. In our LAOLETs, the UV light activated post-synaptic current has fuelled a persistent bright emission with CIE x,y (0.37, 0.57) expanding from the gold electrode with a 270s lifetime. The brightness and lifetime of devices could be enhanced by prolonged UV irradiation, resulting in long-term plasticity of post-synaptic brightness. The decaying ratio could be also modulated by controlling the gate voltage. Finally, large size of 2.5 × 2.5 cm^2 long afterglow light-emitting devices capable to record UV irradiations were also realized, demonstrating the enormous potential of our LAOLETs for applications as visual UV micro-sized sensors. In perspective, our LAOLETs is a promising functional element for the development of active-matrix integrated displays and optical memories.

Supporting Information

Supporting Information is available from the Wiley Online Library or from the author.

Acknowledgements

This work was financially supported by the Labex project CSC (ANR-10-LABX-0026 CSC) within the Investissement d'Avenir program ANR-10-IDEX-0002-02, the International Center for Frontier Research in Chemistry (icFRC), the Institut Universitaire de France (IUF) and the Chinese Scholarship Council.

Received: ((will be filled in by the editorial staff))
Revised: ((will be filled in by the editorial staff))
Published online: ((will be filled in by the editorial staff))

Conflict of Interest

The authors declare no conflict of interest.

References

[1] a) X. Y. Chin, D. Cortecchia, J. Yin, A. Bruno, C. Soci, *Nat. Commun.* **2015**, *6*, 7383; b) R. Capelli, S. Toffanin, G. Generali, H. Usta, A. Facchetti, M. Muccini, *Nat. Mater.* **2010**, *9*, 496; c) L. Hou, X. Zhang, G. F. Cotella, G. Carnicella, M. Herder, B. M. Schmidt, M. Patzel, S. Hecht, F. Cacialli, P. Samorì, *Nat. Nanotechnol.* **2019**, *14*, 347; d) Z. Qin, H. Gao, J. Liu, K. Zhou, J. Li, Y. Dang, L. Huang, H. Deng, X. Zhang, H. Dong, W. Hu, *Adv. Mater.* **2019**, *31*, 1903175; e) K. Muhieddine, M. Ullah, B. N. Pal, P. Burn, E. B. Namdas, *Adv. Mater.* **2014**, *26*, 6410; f) K. Muhieddine, M. Ullah, F. Maasoumi, P. L. Burn, E. B. Namdas, *Adv. Mater.* **2015**, *27*, 6677. g) J. Zaumseil and H. Sirringhaus, *Chem. Rev.* **2007**, *107*, 1296-1323. h) J. Zaumseil, R. H. Friend, H. Sirringhaus, *Nat. Mater.* **2006**, *5*, 69–74.

[2] a) H. Uoyama, K. Goushi, K. Shizu, H. Nomura, C. Adachi, *Nature* **2012**, *492*, 234; b) S. Hirata, Y. Sakai, K. Masui, H. Tanaka, S. Y. Lee, H. Nomura, N. Nakamura, M. Yasumatsu, H. Nakanotani, Q. Zhang, K. Shizu, H. Miyazaki, C. Adachi, *Nat. Mater.* **2015**, *14*, 330; c) H. Nakanotani, T. Higuchi, T. Furukawa, K. Masui, K. Morimoto, M. Numata, H. Tanaka, Y. Sagara, T. Yasuda, C. Adachi, *Nat. Commun.* **2014**, *5*, 4016; d) B. Barnes, *Nat. Photonics* **2021**, *15*, 169; e) S. O. Jeon, K. H. Lee, J. S. Kim, S.-G. Ihn, Y. S. Chung, J. W. Kim, H. Lee, S. Kim, H. Choi, J. Y. Lee, *Nat. Photonics* **2021**, *15*, 208.

[3] L. Song, Y. Hu, Z. Liu, Y. Lv, X. Guo, X. Liu, *ACS Appl. Mater. Interfaces* **2017**, *9*, 2711.

[4] a) W. Zhao, Z. He, B. Z. Tang, *Nat. Rev. Mater.* **2020**, *5*, 869; b) S. Xu, R. Chen, C. Zheng, W. Huang, *Adv. Mater.* **2016**, *28*, 9920.

[5] a) X. Yang, D. Yan, *Adv. Opt. Mater.* **2016**, *4*, 897; b) Y. Katsurada, S. Hirata, K. Totani, T. Watanabe, M. Vacha, *Adv. Opt. Mater.* **2015**, *3*, 1726; c) S. Wang, D. Wu, S. Yang, Z. Lin, Q. Ling, *Mater. Chem. Front.* **2020**, *4*, 1198; d) L. Xu, K. Zhou, H. Ma, A. Lv, D. Pei, G. Li, Y. Zhang, Z. An, A. Li, G. He, *ACS Appl. Mater. Interfaces* **2020**, *12*, 18385; e) C. Xie, X. Zhen, Q. Miao, Y. Lyu, K. Pu, *Adv. Mater.* **2018**, *30*, 1801331; f) Z. An, C. Zheng, Y. Tao, R. Chen, H. Shi, T. Chen, Z. Wang, H. Li, R. Deng, X. Liu, W. Huang, *Nat. Mater.* **2015**, *14*, 685.

[6] R. Kabe, N. Notsuka, K. Yoshida, C. Adachi, *Adv. Mater.* **2016**, *28*, 655.

[7] a) J. Jang, Y. Hong, *Thin Solid Films* **2020**, *707*, 138098; b) S. Lee, A. Nathan, S. Jeon, J. Robertson, *Sci. Rep.* **2015**, *5*, 14902; c) S. Jeon, S. E. Ahn, I. Song, C. J. Kim, U. I. Chung, E. Lee, I. Yoo, A. Nathan, S. Lee, J. Robertson, K. Kim, *Nat. Mater.* **2012**, *11*, 301.

[8] a) M. K. Kim, J. S. Lee, *Adv. Mater.* **2020**, *32*, 1907826; b) J. T. Yang, C. Ge, J. Y. Du, H. Y. Huang, M. He, C. Wang, H. B. Lu, G. Z. Yang, K. J. Jin, *Adv. Mater.* **2018**, *30*, 1801548; c) J. Sun, S. Oh, Y. Choi, S. Seo, M. J. Oh, M. Lee, W. B. Lee, P. J. Yoo, J. H. Cho, J.-H. Park,

Adv. Funct. Mater. **2018**, *28*, 1804397; d) L. Q. Zhu, C. J. Wan, L. Q. Guo, Y. Shi, Q. Wan, *Nat. Commun.* **2014**, *5*, 3158.

[9] a) M. K. Kim, J. S. Lee, *Nano Lett.* **2019**, *19*, 2044; b) Y. Zhou, J. Li, Y. Yang, Q. Chen, J. Zhang, *ACS Appl. Mater. Interfaces* **2020**, 12, 980; c) L. Chen, L. Wang, Y. Peng, X. Feng, S. Sarkar, S. Li, B. Li, L. Liu, K. Han, X. Gong, J. Chen, Y. Liu, G. Han, K. W. Ang, *Adv. Electron. Mater.* **2020**, *6*, 2000057; d) C. S. Yang, D. S. Shang, N. Liu, G. Shi, X. Shen, R. C. Yu, Y. Q. Li, Y. Sun, *Adv. Mater.* **2017**, *29*, 1700906; e) A. A. Bessonov, M. N. Kirikova, D. I. Petukhov, M. Allen, T. Ryhanen, M. J. Bailey, *Nat. Mater.* **2015**, *14*, 199. f) H. Han, H. Yu, H. Wei, J. Gong, W. Xu, *Small* **2019**, *15*, 1900695. g) H.-L. Park, H. Kim, D. Lim, H. Zhou, Y.-H. Kim, Y. Lee, S. Park, T.-W. Lee, *Adv. Mater.* **2020**, *32*, 1906899.

[10] T.-L. Wu, M.-J. Huang, C.-C. Lin, P.-Y. Huang, T.-Y. Chou, R.-W. Chen-Cheng, H.-W. Lin, R.-S. Liu, C.-H. Cheng, *Nat. Photonics* **2018**, *12*, 235.

[11] Q. Wu, J. Wang, J. Cao, C. Lu, G. Yang, X. Shi, X. Chuai, Y. Gong, Y. Su, Y. Zhao, N. Lu, D. Geng, H. Wang, L. Li, M. Liu, *Adv. Electron. Mater.* **2018**, *4*, 1800556.

[12] M. Lee, W. Lee, S. Choi, J. W. Jo, J. Kim, S. K. Park, Y. H. Kim, *Adv. Mater.* **2017**, *29*, 1700951.

[13] M. Di Lauro, A. De Salvo, G. C. Sebastianella, M. Bianchi, S. Carli, M. Murgia, L. Fadiga, F. Biscarini, *ACS Appl. Electron. Mater.* **2020**, *2*, 1849.

[14] J. Yu, K. Javaid, L. Liang, W. Wu, Y. Liang, A. Song, H. Zhang, W. Shi, T. C. Chang, H. Cao, *ACS Appl. Mater. Interfaces* **2018**, *10*, 8102.

[15] S. Scholz, D. Kondakov, B. Lüssem, K. Leo, *Chem. Rev.* **2015**, *115*, 8449–8503.

[16] a) O. Bolton, K. Lee, H. J. Kim, K. Y. Lin, J. Kim, *Nat. Chem.* **2011**, *3*, 205; b) S. Hirata, K. Totani, J. Zhang, T. Yamashita, H. Kaji, S. R. Marder, T. Watanabe, C. Adachi, *Adv. Funct. Mater.* **2013**, *23*, 3386.

[17] C. Y. K. W. J. Nam, J. H. Lee , S. G. Park , M. K. Han, *SID Symp. Dig. Tech. Pap.* **2012**, *36*, 1456.

[18] a) C. Wu, T. W. Kim, H. Y. Choi, D. B. Strukov, J. J. Yang, *Nat. Commun.* **2017**, *8*, 752; b) F. S. Yang, M. Li, M. P. Lee, I. Y. Ho, J. Y. Chen, H. Ling, Y. Li, J. K. Chang, S. H. Yang, Y. M. Chang, K. C. Lee, Y. C. Chou, C. H. Ho, W. Li, C. H. Lien, Y. F. Lin, *Nat. Commun.* **2020**, *11*, 2972.

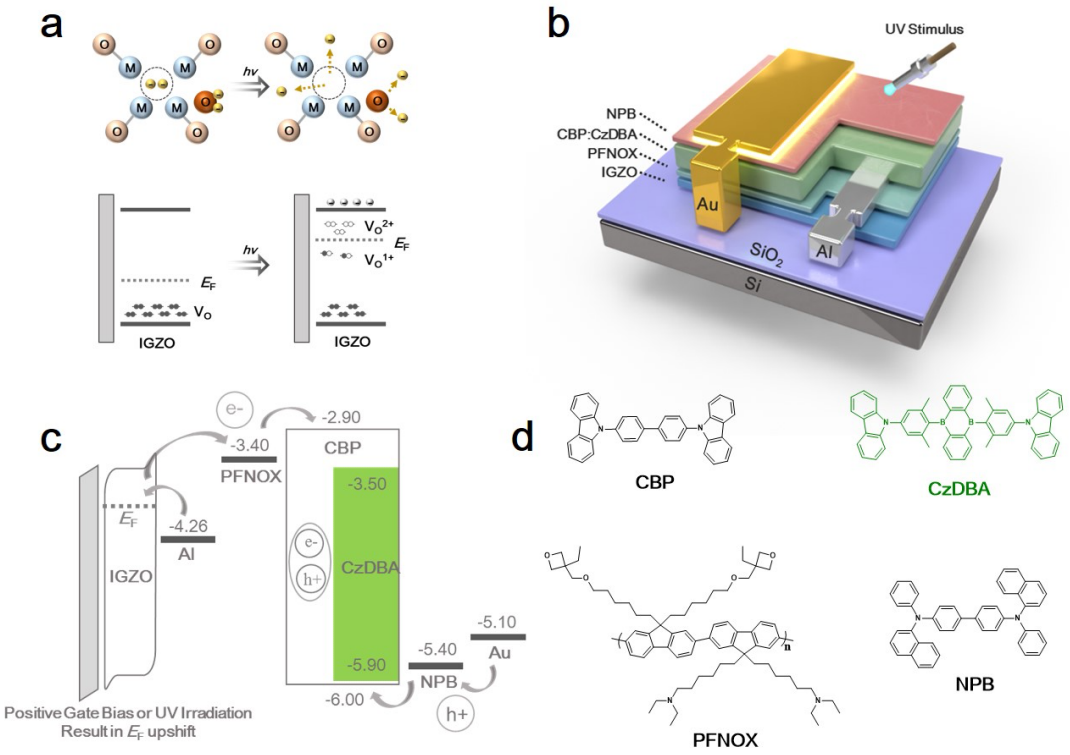

Figure 1. Schematic images of work mechanism and device structure of LAOLETs. a) Schematic illustration of the mechanism of PPC phenomenon. b) Device structure of LAOLETs. c) Energy levels and d) chemical structures of CBP, CzDBA, PFNOX, and NPB.

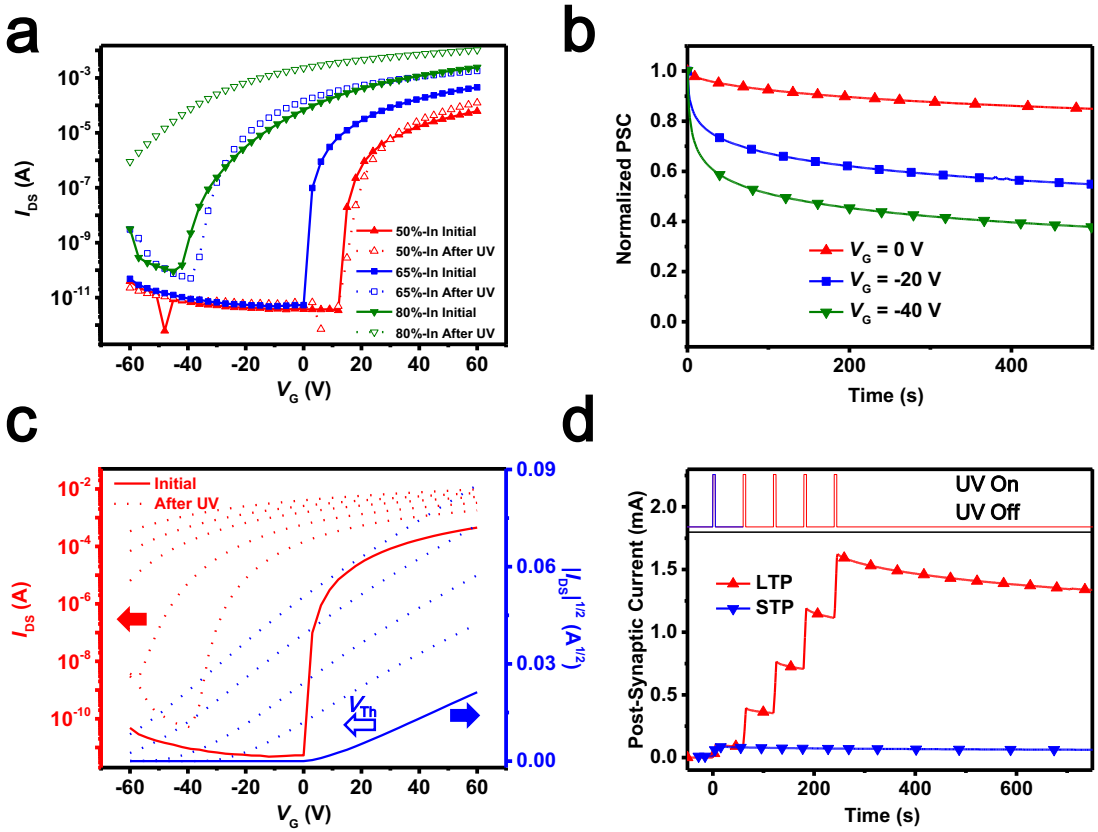

Figure 2. Basic synaptic properties of IGZO FET. a) Transfer curves for 50%-, 65%- and 80%-In IGZO-based transistors. b) Time dependent measurement of normalized PSC when different gate voltage applied. c) Transfer curves for 65%-In IGZO-based transistors before and after five times 5 s UV irradiation. d) Time dependent measurement of 65%-In IGZO-based transistors with five times stimulus and one time stimulus, which show the LTP and STP.

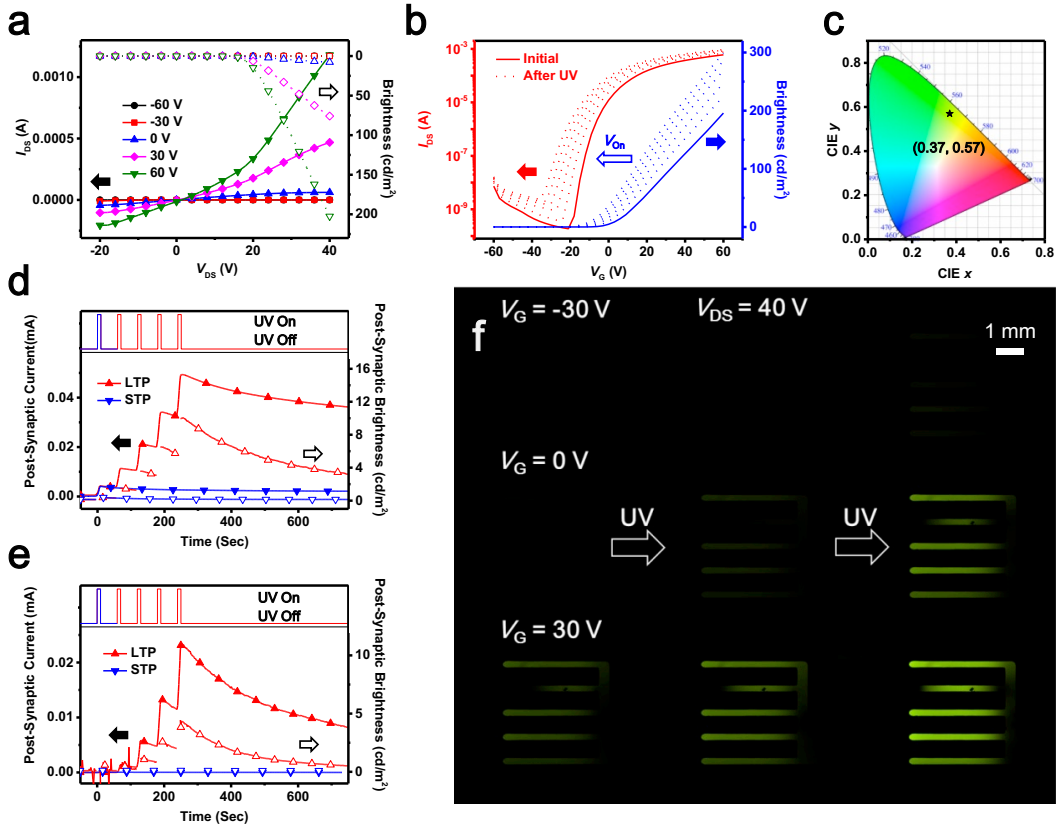

Figure 3. Electrical and optical characterization of LAOLETs. Optical-electrical a) transfer and b) output curves for LAOLETs. c) The corresponding CIE coordinates of electroluminescence spectra. Time dependent measurement of LAOLETs with five times stimulus and one time stimulus, where V_G was d) 0V and e) 30V. f) Typical microscopy images of LAOLETs after twice 20s UV stimulus when V_G with −30V, 0V and 30V were applied.

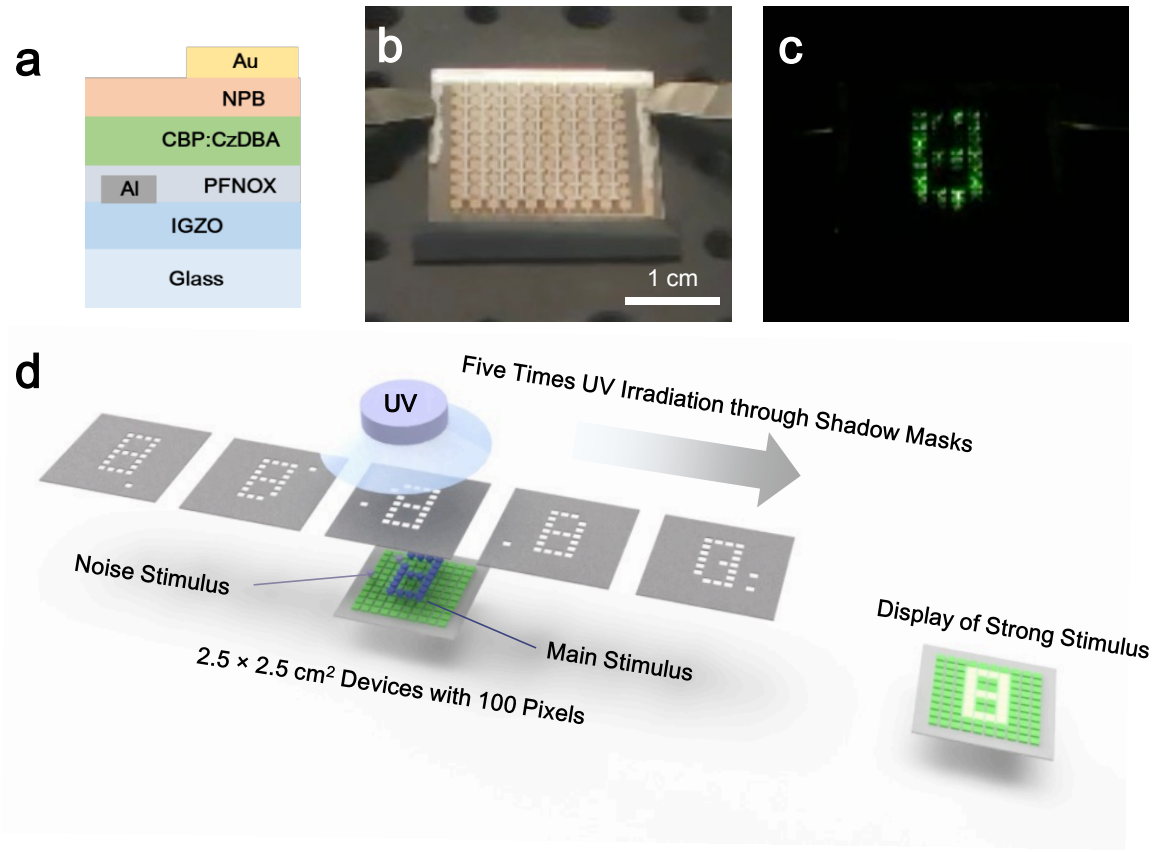

Figure. 4 Typical optical image and schematic images of two terminal long afterglow device with 100 pixels. a) Cross section schematic images of device structure. b) Optical image of device. c) Light emission image of device after five times UV irradiation. d) Schematic illustration of UV irradiation through five different shadow masks which lead to five similar stimuli with different noise, and correct pattern of "8" display finally. V_{DS} of 40 V were applied for this device.

Table 1. Summary of parameter of 65%-In IGZO-based transistor under different times UV irradiation.

	Mobility ($cm^2 V^{-1} s^{-1}$)	V_{Th} (V)	I_{on}/I_{off}
Initial	0.151	4.86	10^7
312nm-5s	0.275	−24.8	10^6
312nm-10s	0.322	−45.8	10^5
312nm-15s	0.331	−71.8	10^3
312nm-20s	0.348	−89.9	10^2
312nm-25s	0.358	−111	10

Table 2. Summary of parameter of LAOLETs under different times UV irradiation.

	Mobility ($cm^2 V^{-1} s^{-1}$)	V_{Th} (V)	V_{On} (V)
Initial	0.128	−12.0	3.0
312nm-10 s	0.130	−16.2	0.3

312nm-20 s	0.130	−20.0	−3.1
312nm-30 s	0.132	−23.2	−5.3
312nm-40 s	0.132	−26.1	−7.5
312nm-50 s	0.129	−29.4	−9.7